

ORIGINAL ARTICLE

## Primary Human Lung Pericytes Support and Stabilize *In Vitro* Perfusable Microvessels

Colette A. Bichsel, MSc,<sup>1,2</sup> Sean R.R. Hall, PhD,<sup>3,4</sup> Ralph A. Schmid, MD, PhD,<sup>3,4</sup> Olivier T. Guenat, PhD,<sup>1-3,\*</sup> and Thomas Geiser, MD, PhD<sup>2,4,\*</sup>

The formation of blood vessels is a complex tissue-specific process that plays a pivotal role during developmental processes, in wound healing, cancer progression, fibrosis, and other pathologies. To study vasculogenesis and vascular remodeling in the context of the lung, we developed an *in vitro* microvascular model that closely mimics the human lung microvasculature in terms of three-dimensional architecture, accessibility, functionality, and cell types. Human pericytes from the distal airway were isolated and characterized using flow cytometry. To assess their role in the generation of normal microvessels, lung pericytes were mixed in fibrin gel and seeded into well-defined microcompartments together with primary endothelial cells (human umbilical cord vein endothelial cells). Patent microvessels covering an area of 3.1 mm<sup>2</sup> formed within 3–5 days and were stable for up to 14 days. Soluble signals from the lung pericytes were necessary to establish perfusability, and pericytes migrated toward endothelial microvessels. Cell–cell communication in the form of adherens and tight junctions, as well as secretion of basement membrane were confirmed using transmission electron microscopy and immunocytochemistry on chip. Direct coculture of pericytes with endothelial cells decreased the microvascular permeability by one order of magnitude from 17.8 × 10<sup>-6</sup> to 2.0 × 10<sup>-6</sup> cm/s and led to vessels with significantly smaller and less variable diameter. Upon phenylephrine administration, vasoconstriction was observed in microvessels lined with pericytes, but not in endothelial microvessels only. Perfusable microvessels were also generated with human lung microvascular endothelial cells and lung pericytes. Human lung pericytes were thus shown to have a prominent influence on microvascular morphology, permeability, vasoconstriction, and long-term stability in an *in vitro* microvascular system. This biomimetic platform opens new possibilities to test functions and interactions of patient-derived cells in a physiologically relevant microvascular setting.

### Introduction

**T**HE ASSEMBLY AND remodeling of vascular structures is highly important during fetal development, wound healing, and cancer progression.<sup>1,2</sup> Vascular dynamics also play a key role in numerous diseases in a tissue-specific manner. In pulmonary arterial hypertension (PAH) for example, vascular remodeling and vasoconstriction of the lung microvasculature lead to an increased pulmonary vascular resistance, decreased vessel compliance, and consequently hypertension.<sup>3</sup> Although some mechanisms that alter the vasculature, such as excessive pericyte proliferation<sup>4</sup> and calcium sensitization have recently been identified, the complex interplay between endothelial cells and pericytes and their combined effects on disease progression are still incompletely understood.<sup>5</sup> Angiogenesis is also believed to play a key role

in idiopathic pulmonary fibrosis (IPF), an aggressive and usually fatal disease.<sup>6</sup> IPF not only damages the alveolar architecture but also affects the pulmonary microvasculature. However, the role of pulmonary angiogenesis in the fibrotic lung, in particular on the temporal and spatial heterogeneity of *de novo* vascularization and vascular degradation, remains controversial.<sup>7</sup>

Advanced *in vitro* systems that closely mimic the conditions of the human lung are one strategy among many to increase our understanding of pulmonary vasculogenesis and vascular remodeling. Recently, several *in vitro* models that reproduce vascular structures have been developed. The group of Stroock micropatterned collagen I gel and lined the 100 μm wide lumens with endothelial cells.<sup>8</sup> These vascular structures were stable and perfusable, but vascular remodeling was limited due to a high gel stiffness. A different

<sup>1</sup>Lung Regeneration Technologies, ARTORG Center, University of Bern, Bern, Switzerland.

<sup>2</sup>Division of Pulmonary Medicine and <sup>3</sup>Division of Thoracic Surgery, University Hospital of Bern, Bern, Switzerland.

<sup>4</sup>Department of Clinical Research, University of Bern, Bern, Switzerland.

\*Shared senior authorship.

approach was taken by Moya *et al.*,<sup>9</sup> who used the vasculogenic properties of endothelial cells under shear stress to initiate vessel formation. Yet another method exploited the natural microvessel formation of endothelial cells inside fibrin gel by providing appropriate growth factors and signals from fibroblasts.<sup>10,11</sup>

These novel models mimic the cellular microenvironment much better than standard *in vitro* assays performed in static conditions. Endothelial cells attach to and modify a three-dimensional (3D) meshwork to form perfusable microvessels and with the addition of perivascular cells or physiological interstitial flow further approach *in vivo*-like conditions. Specifically, perivascular support cells, either fibroblasts<sup>9,10</sup> or mesenchymal stem cells,<sup>12</sup> were shown to positively impact vessel orientation and stabilization, representing inherent functions performed by mural cells *in vivo*. However, in the microvasculature of the lung and organs such as the brain and kidney, pericytes are the main mural cells. In the lung, they are also present around pulmonary capillaries.<sup>13</sup> Apart from their location in the basal membrane around endothelial microvessels, pericytes are identified by surface markers such as NG2, CD146, 3G5,  $\alpha$  smooth muscle actin ( $\alpha$ SMA), and platelet-derived growth factor receptor  $\beta$  (PDGFR $\beta$ ).<sup>14</sup> Pericytes are key players during vessel morphogenesis and in controlling vessel stabilization, remodeling, and tightness. Two recent studies have linked abnormal pericyte coverage to the progression of human PAH<sup>4</sup> and pulmonary fibrosis,<sup>15</sup> respectively, underlining their functional importance in the lung microvasculature.

In this study, our objective was to identify and assess the functional role of primary human lung pericytes and endothelial cells in a microfluidic platform for perfusable microvasculature. In a first phase, the various parameters of the *in vitro* model were established using primary human lung pericytes cocultured with endothelial cells from the umbilical vein. In a second step, primary human lung microvasculature endothelial cells and pericytes were used to more faithfully mimic the lung microvascular environment. Vasculogenesis and pericyte recruitment were observed over days and direct cell–cell interactions were imaged in high resolution. The effects of the pericytes on endothelial cells were investigated using two coculture strategies, by seeding these cells in direct contact or in spatially separated but communicating compartments. Our results show that the direct presence of pericytes around the microvasculature has a dramatic effect on vessel morphology, permeability, and vasoconstriction.

## Materials and Methods

### Device design and fabrication

A 100  $\mu$ m high microfluidic device with five compartments separated by trapezoidal micropillars with 100  $\mu$ m spacing was designed, based on a design reported by Kim and colleagues.<sup>10</sup> Unlike the aforementioned system, the central chamber of the chip was round and wider (2 mm diameter with a central pillar for stability), the adjacent flow channels were 1 mm wide and the outermost chambers 0.5 mm wide. Standard photolithography was used to pattern the microstructures with negative photoresist (GM-1070; Gersteltec) on Si-wafers. Polydimethylsiloxane (PDMS; Sylgard) was mixed at a 10:1 ratio with curing agent, casted on the mold, and cured for at least 2 h at 80°C. Chips were

cut, access ports for gel loading punched with 0.5 mm biopsy punches (Shoney Scientific), and reservoirs with 5 mm punches (AEP Medicalcare). Finally, cleaned chips and standard glass cover slips were activated in oxygen plasma (Harrick Plasma Cleaner) at 650 mTorr for 25 s, bonded together, and baked overnight at 60°C before use.

### Cell culture

Primary human umbilical cord vein endothelial cells (HUVEC PCS-100-010; ATCC) were cultured on 0.1% gelatin-coated flasks in endothelial growth medium 2 (EGM-2) cell culture medium (Lonza). Primary human lung microvascular endothelial cells (HMVEC-L; Lonza) were cultured on 0.1% gelatin-coated flasks in EGM-2 MV cell culture medium (Lonza). Cells between passages 3 and 6 were used for experiments.

### Isolation of lung pericytes

To prospectively isolate lung pericytes, we used lung specimens obtained from patients following surgical resection for lung cancer. Normal tissue was procured from the lung specimen at a distant site of the tumor foci. All patients gave informed written consent for usage of surgical material for research purposes, which was approved by the Ethics Commission of the Canton of Bern, CH.

Preparation of lung tissue and cell sorting was performed as previously described with modifications.<sup>16</sup> Briefly, normal-appearing lung tissue was resected from the tumor foci at a distance >5 cm and digested using a solution of collagenase I and II (Worthington Biochemical Company). Digestion of lung tissue was halted following the addition of 10% fetal bovine serum (FBS; Invitrogen). Single cells were stained with a panel of fluorescently conjugated human monoclonal antibodies directed at the following epitopes: CD45-PB (eBioscience), CD14-PB (eBioscience), CD31-PB (eBioscience), CD235a-PB (eBioscience), CD73-APC (eBioscience), and CD90-FITC (eBioscience). To exclude dead cells, 7-AAD was added before sorting. Cells were sorted using a BD FACS Aria III and were directly cultured in a six-well tissue culture plate precoated with 0.1% gelatin in alpha-minimum essential medium (Sigma) supplemented with 1% FBS (Gibco), 20 ng/mL of recombinant human fibroblast growth factor 2 (Gibco), 25 ng/mL of recombinant human epidermal growth factor (Gibco), 1.25 mg of human insulin (Sigma), and 1% penicillin–streptomycin (Sigma). Cells were grown at 37°C, 5% CO<sub>2</sub>, and low O<sub>2</sub> (3%) until reaching confluence and used up to passage 6. Bone marrow-derived mesenchymal stem cells (BM-MSCs) were isolated using the same antibody and panel as described above.

### Cell characterization

Following expansion, FACS-sorted lung pericytes or BM-MSCs were harvested and resuspended in a FACS staining buffer. Cells were incubated with antibodies on ice and protected from light for 30 min. Following staining, cells were washed and resuspended in phosphate-buffered saline (PBS). Cells were incubated with the following fluorescently conjugated human monoclonal antibodies: PDGFR $\alpha$ -biotin (eBioscience), CD105-FITC (eBioscience), NG2-FITC (eBioscience), CD146-PE (eBioscience), CD61-APC (eBioscience), and CD44-APC (eBioscience). For analysis of

PDGFR $\alpha$ , cells were stained with streptavidin-labeled APC-Cy7 (eBioscience). 7-AAD was added to exclude dead cells and debris. Cell acquisition was performed using a BD FACS LSRII. For analysis, 30,000 events were collected and analyzed using FlowJo software version 10.7 (Treestar).

For transforming growth factor (TGF)- $\beta$ 1 treatment, lung pericytes and BM-MSCs were seeded in eight-well chamber slides. Cells were treated with 10 ng/mL of TGF- $\beta$ 1 (eBioscience) for 3 consecutive days. Thereafter, the cells were washed twice with PBS, fixed with 4% paraformaldehyde (Sigma) for 15 min, washed with PBS, and blocked in a 2% bovine serum albumin (BSA) solution (Sigma) for 1 h. Then, the cells were stained with phalloidin-TRITC (Invitrogen) and  $\alpha$ SMA-FITC (Sigma) and nuclei were counterstained with DAPI for 2 h at room temperature. After washing with PBS, the chamber slides were imaged on a Leica DMI 4000 microscope (10 $\times$  and 20 $\times$  objectives).

#### *Chip loading and maintenance*

Chips were sterilized under UV for 2 h or in an ozone chamber (CoolCLAVE) before loading. Endothelial cells and lung pericytes were resuspended in 2 U/mL thrombin from bovine plasma (Sigma) in EGM-2 at a final concentration of  $2 \times 10^7$  cells/mL (HUVEC),  $1 \times 10^8$  cells/mL (HMVEC-L), and  $1 \times 10^7$  cells/mL, respectively. For combined coculture, the EC and lung pericyte–thrombin suspensions were mixed at a 1:1 ratio, resulting in  $1 \times 10^7$  HUVEC/mL,  $5 \times 10^7$  HMVEC-L/mL, and  $0.5 \times 10^7$  lung pericytes/mL. Fibrinogen from bovine plasma (Sigma) was dissolved in deionized PBS (Gibco) to a concentration of 5 mg/mL. In a separate tube, a clotting test with 2 U/mL thrombin in EGM-2 and 5 mg/mL fibrinogen solution was carried out to confirm clotting of the mixture after 5 min at room temperature. The HUVEC–thrombin suspension was then mixed with 5 mg/mL fibrinogen at a ratio of 1:1 and immediately pipetted into the central chamber. The solution stayed in the central chamber due to liquid pinning between micropillars. Five minutes later, the lung pericyte–thrombin suspension was mixed at a 1:1 ratio with the fibrin solution and injected into the outer chambers. After complete gelation in all chambers (10 min), EGM-2 was pushed through the flow channels and reservoirs were filled. The chips were incubated at 37°C and 5% CO<sub>2</sub> in Petri dishes with a moist tissue for humidification. Cell culture medium was exchanged after 24 h and then every 48 h by emptying all four reservoirs. The reservoirs were filled with medium to create a transient pressure drop across the central chamber with an initial pressure head of 1.3 mm. This hydrostatic pressure enhanced medium supply to the cells in the central chamber. Chips were kept in culture for up to 14 days.

#### *Immunostaining*

The chips were washed twice with PBS, fixed with 4% paraformaldehyde (Sigma) for 15 min, and washed three times with PBS. If intracellular markers were used, 0.1% Triton X-100 (Sigma) was applied for 10 min and washed away 3 $\times$  with PBS. After 1 h of blocking in a 2% BSA (Sigma) solution, primary antibodies VE-cadherin (Santa Cruz), collagen IV (Abcam), PECAM-1 (Santa Cruz),  $\alpha$ SMA (Novus Biological), and ZO-1 (Invitrogen) were incubated overnight at 4°C. Subsequently, devices were washed three times with PBS and incubated with Alexa fluorophore-coupled

secondary antibodies (Molecular Probes), as well as phalloidin (1:100; Invitrogen) and Hoechst (1:1000; Invitrogen) for 2 h at room temperature. After final washings with PBS, the chips were imaged on a Zeiss confocal LSM 710 microscope (10 $\times$ , 20 $\times$ , and 40 $\times$  objectives).

#### *Time-lapse observation*

For time-lapse observations and imaging of endothelial–pericyte interactions, the cells were labeled with lipophilic cell tracker dyes PKH67 green (HUVECs) and PKH26 red (lung pericytes) before seeding. The devices were loaded into the Nikon Biostation CT and imaged every hour with the 4 $\times$  magnification in brightfield, red and green fluorescence. Cell culture medium was replaced every 48 h.

#### *Vascular area and perfusability quantification*

To characterize the vascular networks, z-stacks (10 slices covering a 100  $\mu$ m depth) of tile scans (2.4  $\times$  2.4 mm) of the central chamber were analyzed using the open source image analysis software, Fiji (<http://fiji.sc/Fiji>). The vascularized areas were defined as being phalloidin-positive (separated cocultures in Fig. 5A, B) and PECAM-1-positive (direct cocultures in Fig. 7A). The phalloidin or PECAM-1 signals were quantified from the entire central chamber. The z-stacks were projected on a single plane and binarized with the automatic triangle thresholding method. The binary operation “close” and outlier removal were applied to remove small unconnected particles. “Analyze particles” was used to quantify the vascularized area inside the central chamber. Only areas larger than 100  $\mu$ m in diameter were taken into account to determine the vascularized area percentage. The number of perfusable entrances was assessed visually by checking openings in 3D images obtained with the confocal microscope. Each cell culture condition experiment was repeated three to six times. Average values with standard deviations are reported. Results were compared using a two-tailed Student’s *t*-test.

For measurements of the minimal and maximal diameters, the width of three of the smallest and three of the largest vascular segments (perpendicular to the vessel wall) was measured on tile scans of PKH26-labeled microvessels by using the line and measurement command in Fiji. The mean value and standard deviation of six chips are reported.

#### *Electron microscopy*

The chips were fixed in 2.5% glutaraldehyde (Agar Scientific) in 0.15 M HEPES buffer overnight (total osmolarity: 696 mOsm, pH 7.35), and postfixated for 1 h in a 1% solution of osmium tetroxide (Electron Microscopy Sciences) in 0.1 M sodium cacodylate buffer (total osmolarity: 369 mOsm, pH 7.40). After rinsing in 0.05 M maleate buffer (pH 5.0) the chips were dehydrated in increasing concentrations of ethanol (70%, 80%, 96%, 100%), passed through acetone, and left in a 1:1 mixture of ethanol:epoxy embedding medium (Sigma) overnight. On the following day the chips were filled with epoxy embedding medium and left to polymerize at 60°C for 4 days. Ultrathin sections (70 nm) were cut on a Reichert-Jung Ultracut E microtome, put on formvar-coated 2  $\times$  1 mm single-slot copper grids and double stained with 1% uranyl acetate (Sigma) and 3% lead citrate

(Leica Microsystems). Micrographs were taken in a Philips EM 400 transmission electron microscope.

#### Microbead tracking

Fifty microliters of a yellow fluorescent 1  $\mu\text{m}$  polystyrene bead suspension (Polysciences) was added to one of the four emptied chip reservoirs, generating a pressure head of 1.3 mm. To track individual beads over time, time-lapse images were acquired using a Zeiss confocal LSM 710 at one image per second for 5 min and were analyzed with the TrackMate v2.5.4 plugin in the software Fiji. Bead velocities were added as color map to the images.

#### Microvessel permeability

Seventy kilodaltons rhodamine isothiocyanate (RITC)-coupled dextran (Sigma) at 1 mg/mL in PBS was added to one reservoir. Real-time movies (Panasonic Lumix DMC-LX7) or time-lapse videos (one image every 15 s; Leica DMI 4000) were taken for several minutes. The vascular permeability was calculated as described previously,<sup>17</sup> by measuring fluorescent intensities across vascular segments over time:

$$P = \frac{1}{\Delta I} \frac{dI}{dt} r$$

where  $\Delta I$  is the initial intensity increase when RITC-dextran is added,  $(dI/dt)$  the change of intensity over time due to leakage, and  $r/2$  the volume to area ratio for a cylindrical segment. Three chips ( $n=3$ ) were measured per condition and six to eight regions were quantified per chip. A two-tailed Welch-corrected Student's *t*-test was applied.

#### Vasoactive response quantification

Phenylephrine (Sigma) was dissolved in water (1 mM) and diluted to a concentration of 10  $\mu\text{M}$  in PBS. As control, the equivalent amount of water in PBS was used. After staining the microvasculature with CellMask Orange (Invitrogen) on day 7, 100  $\mu\text{L}$  of the diluted phenylephrine was added into one empty reservoir. A vascular segment was imaged for 5–10 min (Cy3, one image every 10 s; Leica DMI 4000) following drug exposure. The vessel width was assessed over time by measuring the size of a vascular segment (perpendicular to the vessel wall), and plotting a kymograph in Fiji (pixel intensities along the line as a function of time). The vessel walls were identified as the two intensity maxima closest to the image border. The vessel width at each time point was determined as the distance between the two maxima, and normalized to the initial width. Three chips were measured per condition ( $n=3$ ) and five vessel widths were quantified per chip. Results were compared at each time point with a two-tailed Student's *t*-test.

## Results

#### Primary human lung pericyte isolation and characterization

To address the immunophenotypic identity of human lung pericytes *in vivo*, we combined multiple surface markers to prospectively identify putative lung pericytes. As shown in

Figure 1, we identified a cluster of nonhematopoietic (negative for CD45 and CD14), nonendothelial (negative for CD31), and nonepithelial cells (negative for EpCAM) that were positive for key mesenchymal markers CD73 and CD90. When prospectively sorted, these lineage<sup>-</sup>EpCAM<sup>-</sup>CD73<sup>+</sup>CD90<sup>+</sup> cells were spindle shaped resembling pericyte morphology and formed typical colony-forming units (Fig. 1 lower right). Following expansion, the cultured cells were analyzed by multiparameter flow cytometry (Fig. 2A) and shown to highly express the cell adhesion marker integrin beta-3 (ITGB3, CD61), which is involved in binding extracellular matrix proteins. Interestingly, the lung cells demonstrated minimal expression for CD146, a marker found to be highly upregulated on BM-MSCs. Further analysis revealed that the ITGB3<sup>+</sup> lung cells expressed other key pericyte markers NG2 and PDGFR $\alpha$ , whereas on BM-MSCs, PDGFR $\alpha$  was minimally expressed. Moreover, putative lung pericytes were positive for CD105 receptor (endoglin) and CD44, the receptor for hyaluronic acid. To investigate whether these cells are responsive to the pleiotropic cytokine TGF- $\beta$ 1, they were exposed to TGF- $\beta$ 1 for 3 days in culture. TGF- $\beta$ 1-treated cells showed an upregulation in F actin stress fibers using the high affinity probe phalloidin and  $\alpha$ SMA compared to untreated cells (Fig. 2B). Together, these results show that the Lin<sup>-</sup>EpCAM<sup>-</sup>CD73<sup>+</sup>CD90<sup>+</sup> cells isolated from human lungs match the criteria of pericytes, as demonstrated by morphology, the cell surface markers NG2<sup>4</sup> and PDGFR $\alpha$ <sup>18,19</sup> and response to TGF- $\beta$ 1. These cells are thus a suitable choice as perivascular supporting cells for an *in vitro* lung microvascular model.

#### Direct and indirect cocultures in the microfluidic chip

The specific design of the microfluidic chip enabled perfusable microvasculature to form and to investigate the effects of the pericytes on the endothelial vessels (Fig. 3). The microvasculature was formed inside a 100  $\mu\text{m}$  high central chamber of the chip that was filled with cells and fibrin hydrogel. After fibrin polymerization, the two flow channels adjacent to the central chamber were filled with physiological medium. The hydrogel/physiological medium interface enabled molecular diffusion of nutrients, oxygen, and growth factors required for the cells to rearrange and create perfusable vessels. Micropillars situated at the perimeter of the central chamber stopped the spreading of the fibrin gel by holding the hydrogel in place due to liquid pinning by surface tension (Fig. 3C). Two additional compartments situated at 1 mm from the central chamber across both flow channels were filled with fibrin gel and pericytes. To examine the vasculogenic potential of the lung pericytes, two coculture strategies were investigated. The first strategy consisted of an indirect coculture approach, in which endothelial cells were spatially separated from the lung pericytes. Endothelial cells suspended in fibrin solution were seeded into the central chamber, whereas the outer chambers were filled with lung pericytes suspended in fibrin solution. The second strategy was based on a direct coculture of endothelial cells and pericytes in the central chamber. In this approach, pericytes were also cultured in the outer chambers. In both strategies, cells could migrate from the outer chambers toward the central chamber through the hydrogel/physiological medium interfaces or vice versa.

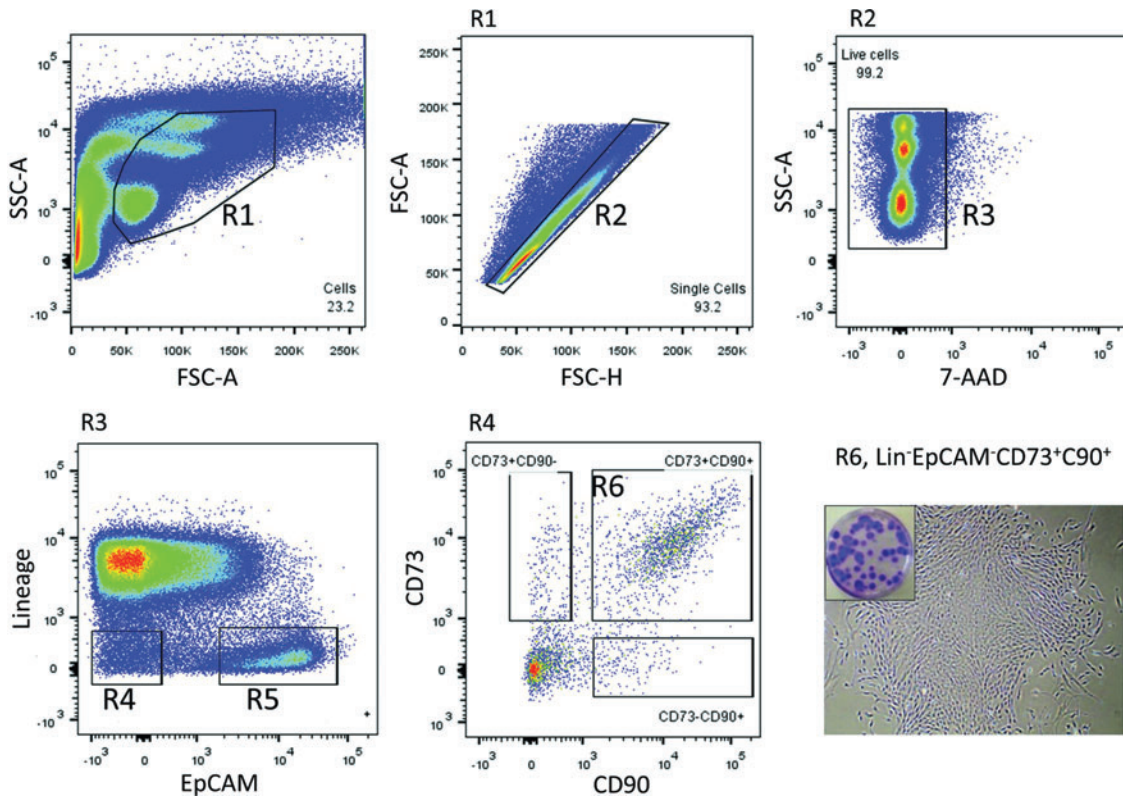


**FIG. 1.** Isolation of putative pericytes from human lung tissue. A subset of small cells was isolated using a six antibody/viability marker panel and polychromatic fluorescence-activated cell sorting. Unfractionated lung cells were initially displayed and gated (R1) on a side scatter-forward scatter pseudocolor density plot, which was subgated to discriminate doublets (R2). Single cells (R2) were further gated to identify live cells that were negative for the dye 7-AAD (gate R3). These cells were subgated onto an antigen plot to display a cluster of lineage-negative ( $\text{Lin}^-$ ; CD45, CD14, CD31 and CD235a) and EpCAM-negative cells (gate R4) and  $\text{Lin}^- \text{EpCAM}^+$  cells (gate R5).  $\text{Lin}^- \text{EpCAM}^-$  cells (R4) were then displayed as a quadrant gate to identify CD73 and CD90 subset of cells. *Lower right:* A representative image of a typical colony-forming unit generated from sorted  $\text{Lin}^- \text{EpCAM}^- \text{CD73}^+ \text{CD90}^+$  cells obtained from gate R6 and higher power image of single colony (4 $\times$ ). Color images available online at [www.liebertpub.com/tea](http://www.liebertpub.com/tea)

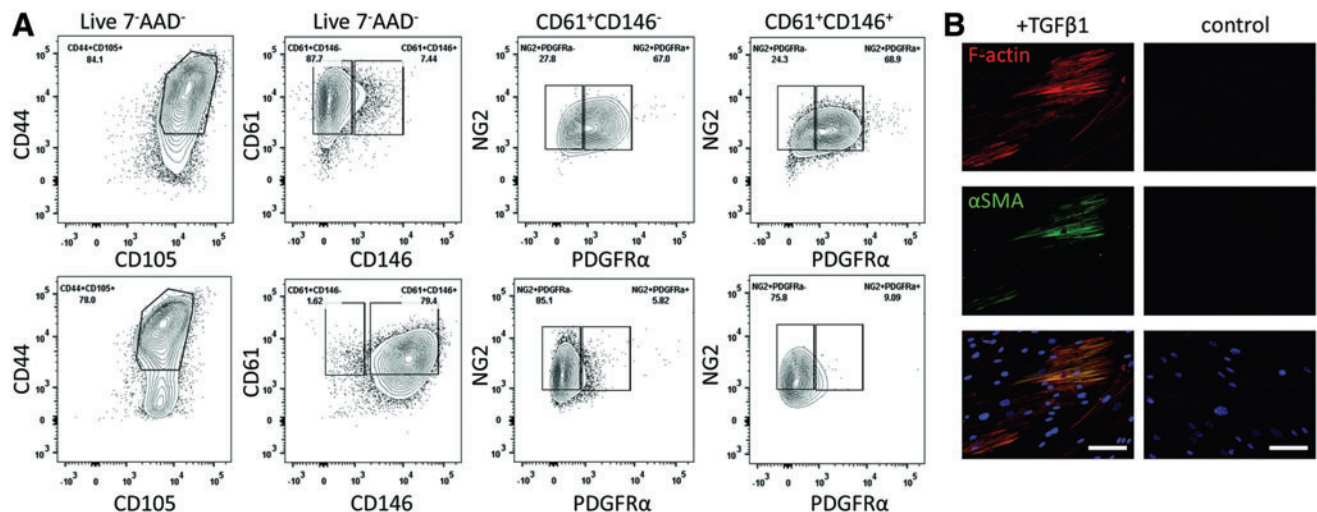


**FIG. 2.**  $\text{Lin}^- \text{EpCAM}^- \text{CD73}^+ \text{CD90}^+$  lung pericyte characterization. (A) Surface marker expression of  $\text{Lin}^- \text{EpCAM}^- \text{CD73}^+ \text{CD90}^+$  cells (*upper panels*) compared to BM-MSC (*lower panels*) by flow cytometry. Representative flow cytometric density plots showing both cell types show high expression of CD44 and CD105 (*first column*). CD146 is highly expressed on BM-MSC, but not on lung pericytes. In both CD146 $^-$  and CD146 $^+$  populations, NG2 and PDGFR $\alpha$  are more highly expressed in lung pericytes than in BM-MSCs. (B)  $\text{Lin}^- \text{EpCAM}^- \text{CD73}^+ \text{CD90}^+$  lung cells were expanded in culture and treated with TGF- $\beta$ 1 (10 ng/mL). F-actin and  $\alpha$ SMA are upregulated compared to vehicle-treated cells. Scale bar: 100  $\mu\text{m}$ . BM-MSC, bone marrow-derived mesenchymal stem cell;  $\alpha$ SMA,  $\alpha$  smooth muscle actin; PDGFR $\alpha$ , platelet-derived growth factor receptor  $\alpha$ ; TGF- $\beta$ 1, transforming growth factor  $\beta$ 1. Color images available online at [www.liebertpub.com/tea](http://www.liebertpub.com/tea)

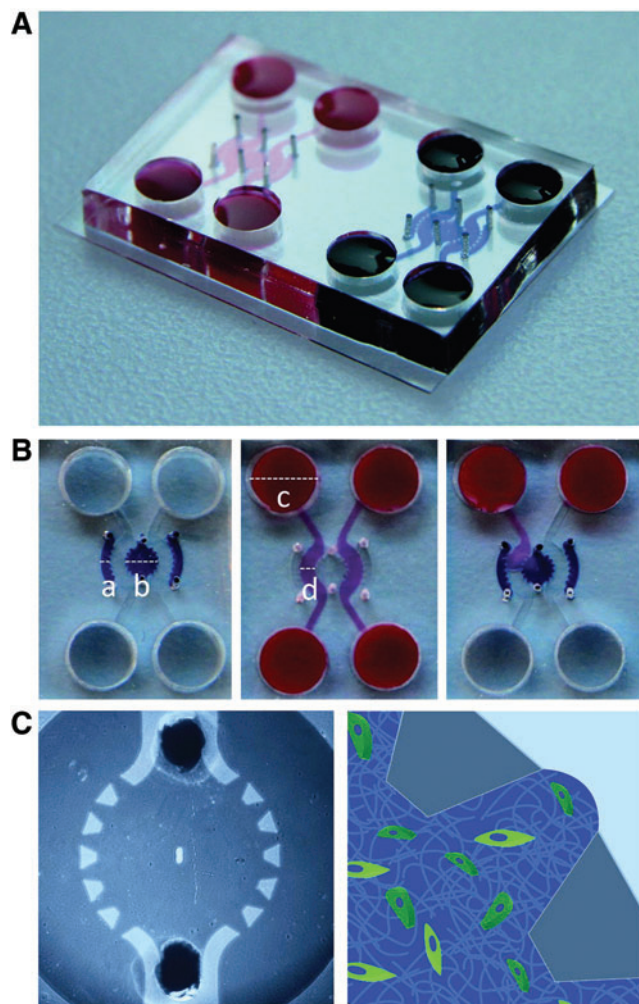


**FIG. 3.** Microfluidic chip specifications. (A) View of a microfluidic chip with two microchannel networks filled with food dye for better visualization. The channels were microstructured in PDMS and bonded on a glass cover slip. (B) Chip loading with hydrogel and cells in the three compartments for cell culture (blue) and with cell culture medium in the two flow channels (red). Dimensions: a, 0.5; b, 2; c, 5; and d, 1 mm. (C) *Left:* Close-up view of the central chamber with 0.5 mm wide inlet and outlet. *Right:* Illustration of the liquid pinning of the fibrin–cell mixture between micropillars of the central compartment. PDMS, polydimethylsiloxane. Color images available online at [www.liebertpub.com/tea](http://www.liebertpub.com/tea)

#### *Lung pericytes support vasculogenesis by paracrine signals*

Following seeding in the central chamber, HUVECs extended toward each other (Fig. 4 and Supplementary Movie S1; Supplementary Data are available online at [www.liebertpub.com/tea](http://www.liebertpub.com/tea)) resulting in vacuole formation, a hallmark of vasculogenesis<sup>20,21</sup> (Fig. 4B top). The process was dynamic with cells fusing, branching, and parting from each other within hours. Vasculogenesis started independently from the spatially separated lung pericytes. After 3–5 days, the overall layout of the vascular segments stabilized, that is, the vessel shape did not dramatically change anymore. However, sprouting events still occurred (Fig. 4B center). Intravascular lumen

grew wider and opened up toward the flow channels between days 4 and 7. In this setting, vascular structures were kept in culture for at least 14 days (Supplementary Fig. S1).

Lung pericytes, originally seeded in a separate outer microcompartment, migrated across the flow channel toward the central chamber and invaded it within 3–5 days (Fig. 4C bottom and Supplementary Movie S1). They slowly migrated through the fibrin gel of the central chamber and aligned along the microvasculature. Importantly, vascular structures only opened up toward the flow channels in the presence of lung pericytes in the outer channel (Supplementary Fig. S2A, B). Cell migration also took place in the opposite direction, whereby HUVECs migrated from the central chamber and moved into the flow channels, thus extending the vascular structure (Supplementary Fig. S3).

#### *In vitro microvessels show typical vascular features and are perfusable*

After 7 days of coculture, patent, interconnected, and perfusable microvessels had formed throughout the 2 mm wide central chamber. Vessel widths ranged between 20 and 220  $\mu\text{m}$ . On average,  $55.4\% \pm 11.0\%$  of the central chamber was covered by vascular structures, and  $73.5\% \pm 13.3\%$  entrances were opened, connecting the microvascular network with the flow channels ( $n=17$ ) (Fig. 5A, B). The mean vascularized area percentage obtained from three independent experiments was  $52.0\% \pm 4.3\%$  ( $n=6$  chips),  $61.1\% \pm 16.2\%$  ( $n=6$ ), and  $52.7\% \pm 7.5\%$  ( $n=5$ ). The variation between experiments was not significant ( $p=0.31$ ), thus the vascular structures formed in a reproducible manner. Likewise, the percentage of perfusable entrances was comparable between experiments with  $72.2 \pm 8.6\%$  ( $n=6$ ),  $73.6\% \pm 19.3\%$  ( $n=6$ ), and  $75.0\% \pm 11.8\%$  ( $n=5$ ) ( $p=0.95$ ). When EGM-2 was replaced only every 48 h as compared to every 24 h, the vascularized area percentage decreased from  $63.1\% \pm 3.2\%$  ( $n=5$ ) to  $52.0\% \pm 4.3\%$  ( $n=6$ ) ( $p=0.001$ ), and there were less perfusable entrances ( $83.3\% \pm 5.9\%$  ( $n=5$ ) compared to  $72.2\% \pm 8.6\%$  ( $n=6$ ) ( $p=0.037$ ) (Fig. 5A).

Immunostainings for VE-cadherin and PECAM-1/CD31 confirmed the presence of adherens junctions between the endothelial cells building the microvessels (Fig. 5C). Furthermore, ZO-1 confirmed the presence of tight junctions along all vessels. Most importantly, microvessels secreted basement membrane components on the basolateral side, as confirmed by collagen IV staining. Tight association between the endothelial cells of a microvessel was also confirmed with transmission electron microscopy (Fig. 5D right). Furthermore, pericytes were only found on the abluminal side, often in close contact with the microvasculature (Fig. 5D left).

Perfusability is one of the key features of a functional vasculature. To confirm accessibility of the microvessels from the flow channels, a suspension of fluorescent polystyrene microspheres (1  $\mu\text{m}$  diameter) was loaded in one reservoir, generating an initial pressure drop of 1.3 mm across the central chamber. Indeed, microbeads flowed through accessible vascular segments (Fig. 5E and Supplementary Movie S2). Under these flow conditions the mean bead velocity was  $6.8 \mu\text{m/s}$  with minimum and maximum speeds comprised between  $0 \mu\text{m/s}$  at the border of the vessels and up to  $20 \mu\text{m/s}$  in the center (Supplementary Fig. S4). The

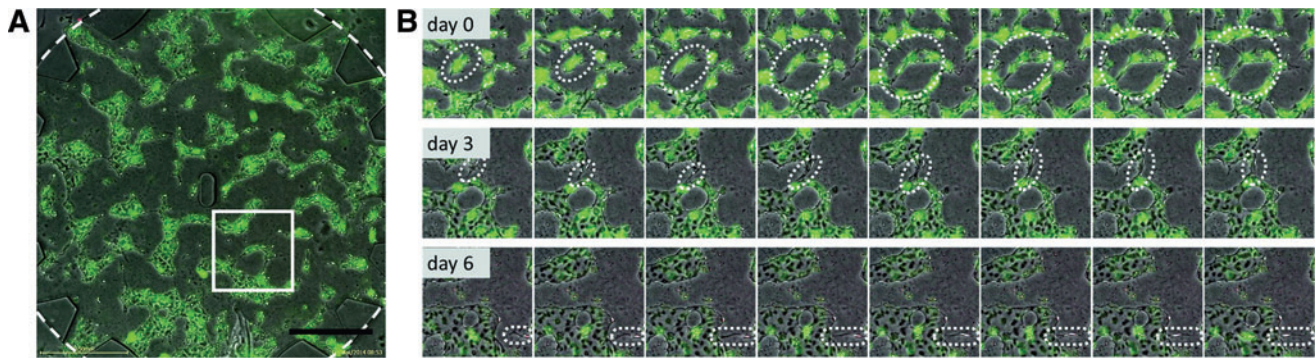


**FIG. 4.** Vasculogenesis in the microfluidic chip. PKH67 (green)-labeled HUVECs were seeded into the central chamber, and PKH26 (red)-labeled pericytes were seeded into the side chambers, and vasculogenesis was observed with time-lapse imaging for 7 days. **(A)** View of the central chamber (inside dotted circle) on day 2. Endothelial cells arrange to form tube-like structures throughout the central chamber. Scale bar: 500  $\mu\text{m}$ . **(B)** Close-up views of a chip segment, focusing on three events during the observation period, interval between images is 1 h. Structures of interest lie inside the dotted line. *Top:* Sprouting, vacuole formation, and lumen fusion of an endothelial cell cluster with neighboring cells. *Center:* Sprouting of an existing vessel toward another vessel, connection, and lumen formation. *Bottom:* Migration of a pericyte toward a vascular structure. HUVECs, human umbilical cord vein endothelial cells. Color images available online at [www.liebertpub.com/tea](http://www.liebertpub.com/tea)

flow path through the microvasculature was also visualized by adding RITC-dextran (Supplementary Movie S3).

#### *Direct coculture with lung pericytes alters vascular morphology, permeability, and vasoactive response*

To observe the effects of direct coculture between lung pericytes and HUVECs, both cell types were mixed and seeded in the central chamber. Lung pericytes were also seeded in the outer chambers to enable vessel opening. The resulting vessel morphology was strikingly different to the separated coculture setting. In direct coculture (Fig. 6A top), vascular diameters were smaller and more streamlined as compared to the separated coculture that had more tortuous vessels (Fig. 6A bottom). Indeed, the measurements of the smallest and largest diameters were significantly smaller for the direct coculture than the separated coculture ( $p=0.005$  for the smallest and  $p<0.001$  for the largest diameter, Table 1). Vessel diameters were also more narrowly distributed in the direct coculture (difference from smallest to largest diameter 116.7  $\mu\text{m}$ ) than the separated coculture (198.6  $\mu\text{m}$ ). Furthermore, immunostaining revealed that some pericytes lining the abluminal side of the microvessels highly expressed  $\alpha\text{SMA}$  (Fig. 6C). In addition to the morphological differences, the vascular integrity was also altered. Perfusion with 70 kDa RITC-coupled dextran filled the vascular structures, but leaked into the interstitial space in the separated coculture setting (Fig. 6B, arrow), whereas no leakage from vessels was obvious in the direct coculture. The calculated permeability coefficients were  $17.8 \times 10^{-6}$  and  $2.0 \times 10^{-6}$  cm/s for the separated and direct coculture, respectively (Table 1). Thus, the direct presence of pericytes lowers the permeability by a factor of 8 ( $p=0.057$ ).

To assess the physiological functionality of the pericytes on *in vitro* microvasculature, we perfused the vasoactive  $\alpha_1$  adrenergic receptor agonist phenylephrine through microvessels in direct and separated cocultures. The direct presence of pericytes influenced the response to phenylephrine. Microvessels with pericyte lining constricted immediately upon phenylephrine administration ( $p<0.05$  between 120 and 300 s,  $n=3$  chips per condition) compared to adminis-

tration of the vehicle (Fig. 6E and Supplementary Fig. S5). No significant difference between phenylephrine and the vehicle was observed in the separated coculture.

#### *Microvasculature with primary human lung-derived cells only*

To mimic the microvasculature of the lung more closely, we replaced HUVECs with HMVEC-Ls. Similarly to HUVECs, HMVEC-Ls assembled to form continuous microvascular networks, surrounded by and supported with lung pericytes. In contrast to direct coculture of HUVEC and lung pericytes, the seeding ratio for HMVEC-L and lung pericytes needed to be increased from 2:1 to 10:1 to promote perfusable microvessels. At lower seeding ratios, the pericytes were more prone to block openings toward the flow channel and impede perfusability. Microvasculature made of primary lung-derived endothelial cells and pericytes covered  $47.74\% \pm 6.05\%$  of the central chamber area on day 5, and  $62.5\% \pm 14.43\%$  of entrances were perfusable ( $n=4$ ). The vessels expressed PECAM-1 and VE-cadherin, showed patent and perfusable lumen, and pericytes were found on the abluminal vessel side exclusively, in close proximity to the endothelial cells (Fig. 7).

## Discussion

Microfabrication technologies applied to vascular biology open new possibilities to study the fascinating processes of vasculogenesis, angiogenesis, and vascular remodeling. Not only can such new experimental platforms address fundamental questions in vasculogenesis, but they may also be used in the future to vascularize tissues before implantation<sup>22</sup> or optimize drug treatments on personalized vasculature models.

Although several studies recently reported on vasculogenesis on chip,<sup>9,10</sup> none focused on reproducing tissue-specific microvasculature with well-defined cell types. To mimic the microvasculature of the lung parenchyma, primary pericytes from human lung parenchyma were used in this study. These cells were prospectively sorted from human lung samples

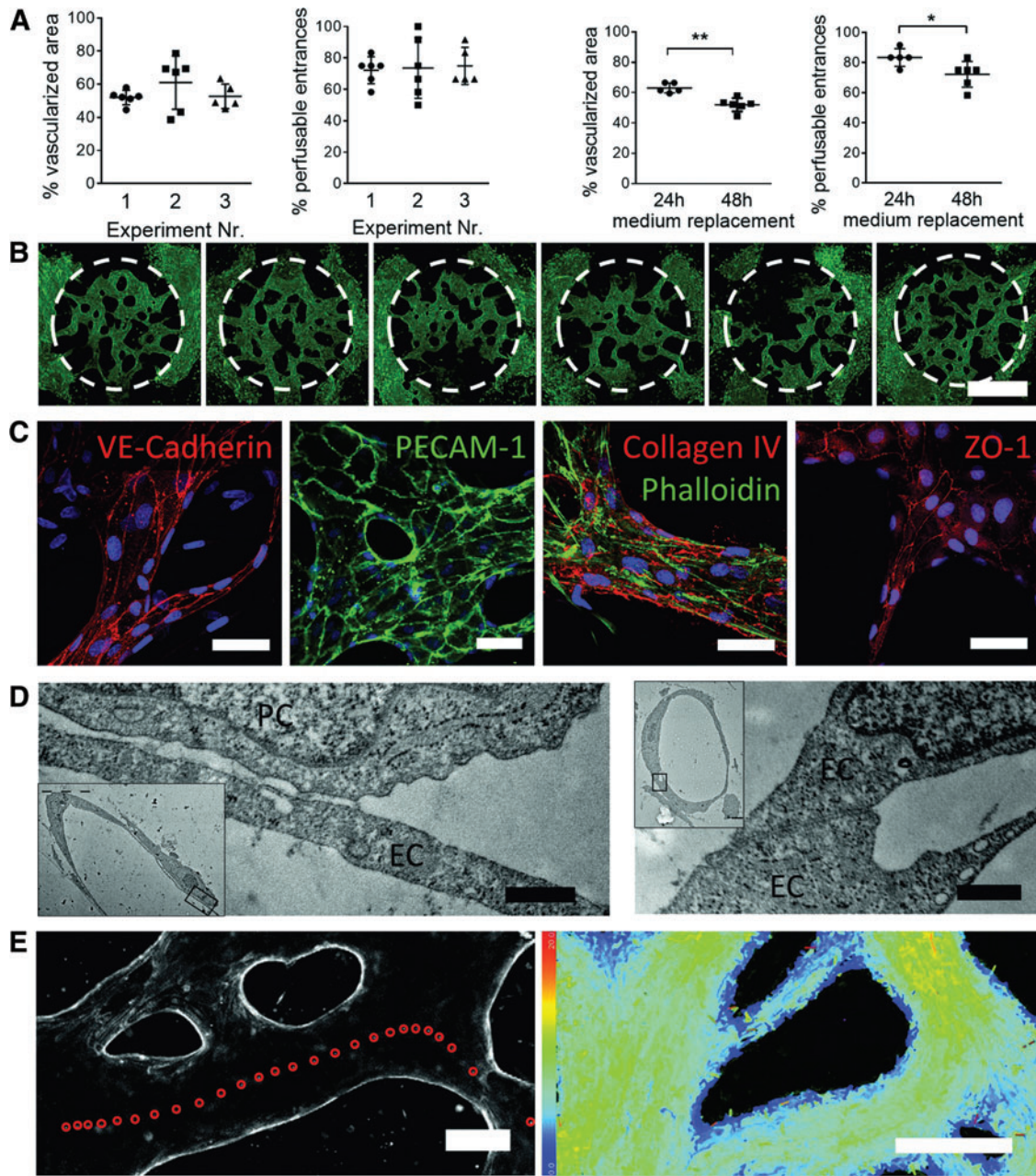


**FIG. 5.** Microvessel characterization on day 7. (A) *Left:* Vascularized area and perfusability are reproducible between three independent vasculogenesis experiments ( $p=0.34, 0.99, 0.45$ ). *Right:* Replacing the medium every 24 h compared to 48 h lead to a higher vascularized area (\*\* $p<0.01$ ) and perfusable entrances (\* $p<0.05$ ). (B) Phalloidin-stained microvasculature after 7 days in six different chips. The delineation marks the central chamber. Scale bar: 1 mm. (C) Microvessels express the adherens junction markers VE-cadherin and PECAM-1, tight junction marker ZO-1, and secrete collagen IV on the basolateral side. Scale bars: 50 μm. (D) Transmission electron micrographs show close association of pericytes with the microvessels (*left*) and junctions between two endothelial cells of a microvessel (*right*). Scale bars: 500 nm. *Insets:* Low-magnification views. (E) *Left:* Overlay of time-lapse images show beads moving inside the vascular lumen and follow the vessel shape, recording frequency is one image per second. Scale bar: 100 μm. *Right:* Color-coded tracks of individual microbeads inside the microvasculature according to local velocities (color range: 0–20 μm/s). Note lower velocities close to the vessel borders. Scale bar: 200 μm. Color images available online at [www.liebertpub.com/tea](http://www.liebertpub.com/tea)

using mesenchymal surface markers while being devoid of known hematopoietic, endothelial, and epithelial markers. The selected cells expressed pericyte-associated cell surface markers and upregulated αSMA upon stimulation with TGF-β1. Interestingly, pericyte surface markers<sup>4,14,18</sup> were more highly expressed in the lung pericytes than the BM-MSCs,

underscoring their specialized function as mural support cells. Taken together, these results confirm that the sorted cell type possess phenotypic and functional characteristics known to be found in pericytes.

To study their role in the context of microvessel assembly and function, the lung pericytes were seeded into the

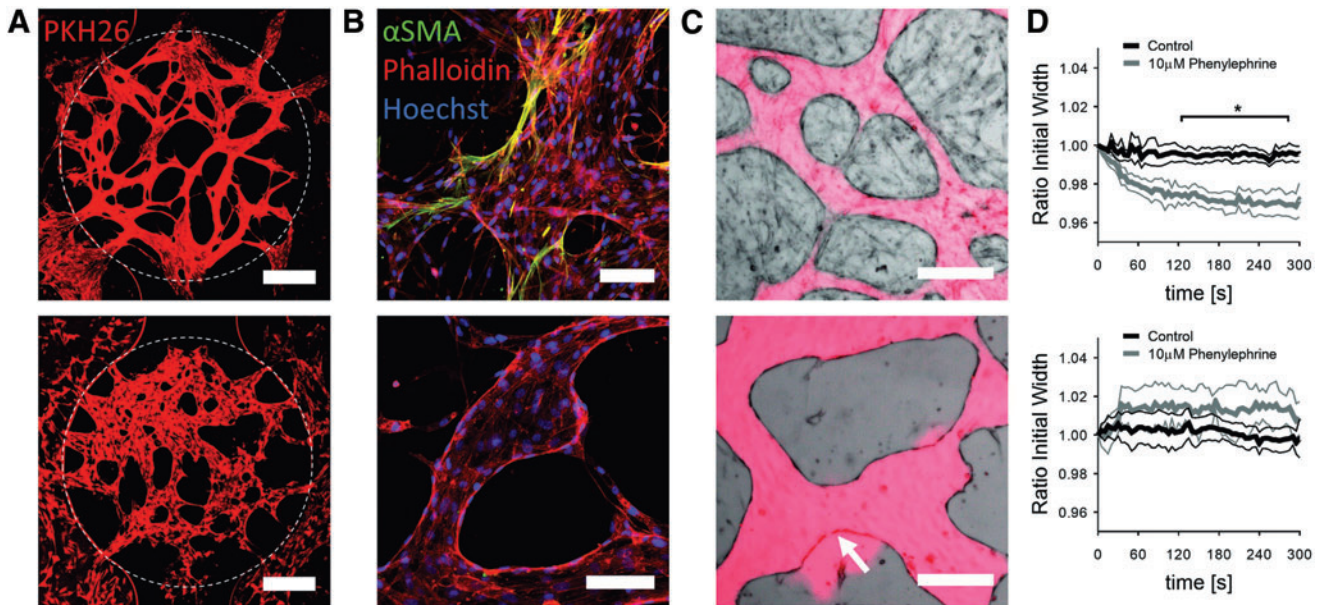


**FIG. 6.** The direct presence of pericytes affects vessel morphology, permeability, and response to phenylephrine. Experiments were carried out on day 7 on direct cocultures (*top row*) or separated cocultures (*lower row*). **(A)** Representative images of vascular morphology visualized by PKH26 perfusion shows less tortuous vessels when pericytes are directly present. Scale bars: 500  $\mu\text{m}$ . **(B)** Some pericytes in direct contact with the microvasculature are  $\alpha\text{SMA}$  positive. Scale bars: 200  $\mu\text{m}$ . **(C)** Perfusion with 70 kDa RITC-labeled dextrane shows focal leaks only in vessels without pericyte coverage (*arrow*). Scale bars: 100  $\mu\text{m}$ . **(D)** Vessel width in response to 10  $\mu\text{M}$  phenylephrine decreased in case of direct ( $*p < 0.05$ , *upper graph*), but not separated coculture (*lower graph*). Mean  $\pm$  SD of  $n = 3$  chips per condition. RITC, rhodamine isothiocyanate. Color images available online at [www.liebertpub.com/tea](http://www.liebertpub.com/tea)

microfluidic platform together with endothelial cells. The different seeding options allowed to separately observe paracrine and direct contact interactions of lung pericytes and ECs. Not surprisingly, the presence of lung pericytes in the chip was necessary for long-term vessel stabilization.<sup>21,23,24</sup> Of note, it was sufficient to seed the two cell types at 1 mm distance from each other to obtain stable vascularization. Over time, both cell types migrated across the separating channel and lung pericytes started to wrap around newly formed vascular segments. The influence of lung pericyte signals on vessel orientation was evident, because vascular segments only opened up toward the flow channel if pericytes were present on the opposing side. This observation shows not only pericyte recruitment during vascular formation, but also reorientation of endothelial neovessels according to pericyte location. The vascular development was also influenced by the growth factors contained in the EGM-2 medium, as shown by the increased area and opened

segments when new media were supplied every day compared to every second day.

In addition to the pericyte recruitment toward the vasculature, we also observed dramatic differences between the two coculturing strategies. When lung pericytes and ECs were mixed and coseeded from the outset, pericytes spread around microvascular segments but were never observed inside vessel lumens. In this direct contact setup, microvessels were narrower and less tortuous as compared to spatially separated seeding. In addition, vessels with a pericyte lining also showed significantly decreased vascular permeability and no leaks in the vessel walls. In fact, pericyte-lined vessel permeability was similar to values measured in mammalian venules,<sup>25</sup> and eight times lower than permeability of vessels with ECs only. This effect may be linked to increased basement membrane secretion in the direct contact setting,<sup>26</sup> but this needs to be verified in subsequent studies. This finding is also in line with the observation that vessels lacking pericytes are wider, have a more tortuous morphology, and are more prone to rupture.<sup>27,28</sup> Moreover, some pericytes in close contact with the microvessels highly expressed  $\alpha\text{SMA}$ , showing a functional response upon direct contact with endothelial cells. Further investigation is needed to determine the molecular interaction that leads to this upregulation.

Administration of phenylephrine demonstrated the vasoconstrictive activity of pericytes, and is consistent with reports of pulmonary microvascular contraction upon phenylephrine administration *in vivo*.<sup>29</sup> We observed slightly smaller values of constriction (3% change in diameter) compared to the animal model (6% change in diameter). However, the reported values were measured in small pulmonary arterioles

**TABLE 1.** COMPARISON OF VASCULAR DIAMETER AND PERMEABILITY OF DIRECT AND SEPARATED ENDOTHELIAL-PERICYTE COCULTURE ON DAY 7

	<i>Direct coculture</i>	<i>Separated coculture</i>	<i>Significance test p-value</i>
Min D ( $\mu\text{m}$ )	20.5 ( $\pm 3.9$ ), $n = 6$	25.6 ( $\pm 6.0$ ), $n = 6$	0.005
Max D ( $\mu\text{m}$ )	137.2 ( $\pm 31.6$ ), $n = 6$	224.2 ( $\pm 41.8$ ), $n = 6$	<0.001
$p$ ( $\times 10^{-6}$ cm/s)	2.0 ( $\pm 1.0$ ), $n = 3$	17.8 ( $\pm 7.0$ ), $n = 3$	0.057

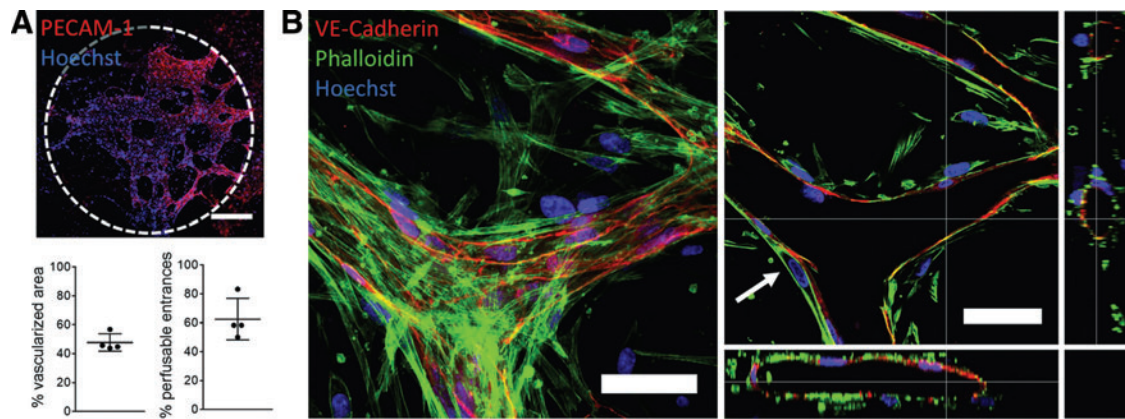


**FIG. 7.** *In vitro* human lung microvasculature. (A) Direct coculture of primary human lung endothelial cells and pericytes lead to perfusable microvessels on day 5, as shown by PECAM-1 staining and quantification of the vascularized area and perfusability (mean  $\pm$  SD). Scale bar: 500  $\mu$ m. (B) HMVEC-L microvessels are lined with pericytes. *Left:* VE-cadherin-positive HMVEC-Ls build a microvessel and are surrounded by VE-cadherin pericytes. *Right:* Cross-sections through the vessel show tight association of pericytes with the microvessel (*arrow*). Scale bars. 50  $\mu$ m. HMVEC-Ls, human lung microvascular endothelial cells. Color images available online at [www.liebertpub.com/tea](http://www.liebertpub.com/tea)

(46  $\mu$ m in diameter) whereas our measurements were performed in larger endothelial vessels (120  $\mu$ m in diameter) covered by pericytes only, thus the two values are not directly comparable. The versatile seeding strategy allowed us to compare the response of vessels made of endothelial cells only and of pericyte-covered endothelial vessels. Interestingly, the former had a slight tendency to enlarge upon fluid loading (both with control and phenylephrine administration), in contrast to the vessels in direct coculture. This observation suggests that pericyte-lined microvessels may possess a higher stiffness compared to endothelial microvessels alone. Taken together, the pericyte functions on microvascular morphology, permeability, and vasoconstriction known from *in vivo* observations were reproduced in our *in vitro* platform and demonstrate the physiological relevance of our system.

In the present study, the final microvasculature was perfusable and covered an area of 3.1 mm<sup>2</sup>. Importantly, the vascular network formation was highly repeatable and resulted in comparable network architecture, despite spontaneous vascular self-assembly. Furthermore, we considered the entire vascular area for analyses, not only selected regions of interest. The longevity, reproducibility, and high area coverage of the perfusable microvasculature may be of interest for future vascularization studies in tissue engineering. In contrast to our results, recent *in vitro* vasculogenesis assays using spatially separated cocultures did not describe recruitment and direct contact of supporting cells with microvessels.<sup>10,11</sup> This might be due to the shorter experimental duration used in these studies. It is also possible that the primary cells used here are more migratory and physiologically relevant as compared to the lung fibroblasts reported earlier.<sup>9,11</sup> In addition, lung resident pericytes might be more specialized in stabilizing microvessels than the less differentiated MSCs.<sup>30</sup>

Traditional *in vitro* assays can measure either permeability (cell seeding on a porous insert) or vasculogenesis (e.g., cell seeding on matrigel), however, there is no readout for vessel morphology of perfusable vessels. In contrast, we can compare vessel morphology, permeability, and marker

expression in the same experiment. This platform is also suitable to perform functional assays that are difficult to carry out in animal models. Recording vasoactive responses of the lung microvasculature *in vivo* is very delicate, and only possible with advanced equipment such as a thoracic window combined with intravital videomicroscopy.<sup>29</sup> In contrast, this readout was straightforward and applicable to human cells in the current platform using fluorescent staining and time-lapse microscopy.

A limitation in our study was the choice of endothelial cells, because HUVECs differ from lung microvascular endothelial cells in terms of gene expression, growth, permeability, and morphology.<sup>31,32</sup> To further increase resemblance of the current *in vitro* model to pulmonary microvessels and capillaries, we therefore used cells from human lung parenchyma exclusively (HMVEC-L and lung pericytes). We demonstrated successful vasculogenesis and the establishment of patent, perfusable microvessels with patient-derived endothelial cells and pericytes from the distal airway. In the future, it is conceivable to test drugs on such models to optimize individual drug treatments for patients suffering from diseases affecting the microvasculature.

## Conclusion

To understand the complex interactions of vascular biology in health and disease, *in vitro* microvascular models must be simple but not reductionist. In this study, we developed an *in vitro* lung microvasculature with prospectively sorted primary pulmonary pericytes and endothelial cells in a microfluidic coculture system. Our setup enabled the formation of microvessels that resembled human lung microvasculature in terms of 3D morphology, vascular marker expression, ultrastructure, permeability, and vasoactive response. To further increase the biological similarity to pulmonary microvessels, human microvascular endothelial cells from the lung were seeded together with lung pericytes and built stable and perfusable microvascular networks. This simple platform enables building tissue- and patient-specific microvascularities amenable to drug testing or modeling of diseases such as PAH.

## Acknowledgments

Special thanks go to Matthieu Delincé for help with photolithography at the Center of MicroNanoTechnology (CMi) at EPFL, Franziska Graber and Adolfo Odriozola for help with transmission electron microscopy, and Prof. Dr. Robert Rieben for discussions and kindly providing endothelial cells. The authors also acknowledge the Microscopy Imaging Center and the FACSLab at the University of Bern.

## Disclosure Statement

No competing financial interests exist.

## References

- Geudens, I., and Gerhardt, H. Coordinating cell behaviour during blood vessel formation. *Development* **138**, 4569, 2011.
- Potente, M., Gerhardt, H., and Carmeliet, P. Basic and therapeutic aspects of angiogenesis. *Cell* **146**, 873, 2011.
- Mandegar, M., *et al.* Cellular and molecular mechanisms of pulmonary vascular remodeling: role in the development of pulmonary hypertension. *Microvasc Res* **68**, 75, 2004.
- Ricard, N., *et al.* Increased pericyte coverage mediated by endothelial-derived fibroblast growth factor-2 and interleukin-6 is a source of smooth muscle-like cells in pulmonary hypertension. *Circulation* **129**, 1586, 2014.
- Budhiraja, R., Tuder, R.M., and Hassoun, P.M. Endothelial dysfunction in pulmonary hypertension. *Circulation* **109**, 159, 2004.
- King, T.E., Pardo, A., and Selman, M. Idiopathic pulmonary fibrosis. *Lancet* **378**, 1949, 2011.
- Hanumegowda, C., Farkas, L., and Kolb, M. Angiogenesis in pulmonary fibrosis: too much or not enough? *Chest* **142**, 200, 2012.
- Zheng, Y., *et al.* In vitro microvessels for the study of angiogenesis and thrombosis. *Proc Natl Acad Sci U S A* **109**, 9342, 2012.
- Moya, M.L., Hsu, Y., Lee, A.P., Hughes, C.C.W., and George, S.C. In vitro perfused human capillary networks. *Tissue Eng Part C Methods* **19**, 730, 2013.
- Kim, S., Lee, H., Chung, M., and Jeon, N.L. Engineering of functional, perfusable 3D microvascular networks on a chip. *Lab Chip* **13**, 1489, 2013.
- Whisler, J.A., Chen, M.B., and Kamm, R.D. Control of perfusable microvascular network morphology using a multiculture microfluidic system. *Tissue Eng Part C Methods* **20**, 543, 2014.
- Jeon, J.S., *et al.* Generation of 3D functional microvascular networks with human mesenchymal stem cells in microfluidic systems. *Integr Biol (Camb)* **6**, 555, 2014.
- Weibel, E.R. On pericytes, particularly their existence on lung capillaries. *Microvasc Res* **8**, 218, 1974.
- Rowley, J.E., and Johnson, J.R. Pericytes in chronic lung disease. *Int Arch Allergy Immunol* **164**, 178, 2014.
- Hung, C., *et al.* Role of lung pericytes and resident fibroblasts in the pathogenesis of pulmonary fibrosis. *Am J Respir Crit Care Med* **188**, 820, 2013.
- Kajstura, J., *et al.* Evidence for human lung stem cells. *N Engl J Med* **364**, 1795, 2011.
- Chrobak, K.M., Potter, D.R., and Tien, J. Formation of perfused, functional microvascular tubes in vitro. *Microvasc Res* **71**, 185, 2006.
- Chen, W.C.W., *et al.* Human myocardial pericytes: multipotent mesodermal precursors exhibiting cardiac specificity. *Stem Cells* **33**, 557, 2015.
- Li, H., *et al.* Low/negative expression of PDGFR- $\alpha$  identifies the candidate primary mesenchymal stromal cells in adult human bone marrow. *Stem Cell Reports* **3**, 965, 2014.
- Xu, K., and Cleaver, O. Tubulogenesis during blood vessel formation. *Semin Cell Dev Biol* **22**, 993, 2011.
- Iruela-Arispe, M.L., and Davis, G.E. Cellular and molecular mechanisms of vascular lumen formation. *Dev Cell* **16**, 222, 2009.
- Rouwkema, J., Rivron, N.C., and van Blitterswijk, C.A. Vascularization in tissue engineering. *Trends Biotechnol* **26**, 434, 2008.
- Armulik, A., Genové, G., and Betsholtz, C. Pericytes: developmental, physiological, and pathological perspectives, problems, and promises. *Dev Cell* **21**, 193, 2011.
- Smith, A.O., Bowers, S.L.K., Stratman, A.N., and Davis, G.E. Hematopoietic stem cell cytokines and fibroblast growth factor-2 stimulate human endothelial cell-pericyte tube co-assembly in 3D fibrin matrices under serum-free defined conditions. *PLoS One* **8**, e85147, 2013.
- Yuan, W., Lv, Y., Zeng, M., and Fu, B.M. Non-invasive measurement of solute permeability in cerebral microvessels of the rat. *Microvasc Res* **77**, 166, 2009.
- Stratman, A.N., Malotte, K.M., Mahan, R.D., Davis, M.J., and Davis, G.E. Pericyte recruitment during vasculogenic tube assembly stimulates endothelial basement membrane matrix formation. *Blood* **114**, 5091, 2009.
- Patel, M.S., *et al.* Abnormal pericyte recruitment as a cause for pulmonary hypertension in Adams-Oliver syndrome. *Am J Med Genet A* **129A**, 294, 2004.
- Hellström, M., *et al.* Lack of pericytes leads to endothelial hyperplasia and abnormal vascular morphogenesis. *J Cell Biol* **153**, 543, 2001.
- McCormack, D.G., *et al.* Pulmonary microvascular changes during sepsis: evaluation using intravital videomicroscopy. *Microvasc Res* **60**, 131, 2000.
- Zannettino, A.C.W., *et al.* Multipotential human adipose-derived stromal stem cells exhibit a perivascular phenotype in vitro and in vivo. *J Cell Physiol* **214**, 413, 2008.
- Chi, J.-T., *et al.* Endothelial cell diversity revealed by global expression profiling. *Proc Natl Acad Sci U S A* **100**, 10623, 2003.
- Craig, L.E., Spelman, J.P., Strandberg, J.D., and Zink, M.C. Endothelial cells from diverse tissues exhibit differences in growth and morphology. *Microvasc Res* **55**, 65, 1998.

Address correspondence to:  
 Olivier T. Guenat, PhD  
 Lung Regeneration Technologies  
 ARTORG Center  
 University of Bern  
 Murtenstrasse 50  
 Postfach 44  
 3010 Bern  
 Switzerland

E-mail: olivier.guenat@artorg.unibe.ch

Received: September 16, 2014

Accepted: April 14, 2015

Online Publication Date: May 27, 2015